Schottky barriers at $NiSi_2$/Si(111) interfaces

Hideaki Fujitani
Fujitsu Laboratories Ltd., 10-1 Morinosato-Wakamiya, Atsugi 243-01, Japan

Setsuro Asano
Institute of Physics, College of Arts and Sciences, University of Tokyo, Komaba, Meguro-ku, Tokyo 153, Japan
(Received 15 February 1989; revised manuscript received 23 February 1990)

The electronic structures of the two types of $NiSi_2$/Si(111) interface were studied within the local-density approximation using the linear muffin-tin orbitals method in the atomic-sphere approximation. Calculations were done for four supercell sizes. The largest supercell contained 12 Si_2 layers and 11 $NiSi_2$ layers. With each large supercell, the difference between the Schottky-barrier heights (SBH's) of the two types of interface was consistent with experimental values. However, SBH's depend on the supercell size, although larger supercells have enough layers to screen the interface disturbance. Why SBH's depend on the cell size is investigated.

I. INTRODUCTION

Metal-semiconductor interfaces play very important roles in modern electronics and microelectronic devices. Their properties have been studied by many groups for years, but the basic question of how Schottky barriers (SB's) form remains unsolved. In 1942, Schottky proposed his model relating the Schottky-barrier height (SBH) to the difference between the metal work function and the electron affinity in the semiconductor.[1] Schottky's model contradicted early experimental evidence, and Bardeen suggested that the Fermi levels are pinned by intrinsic semiconductor surface states.[2] In 1965, Heine pointed out that intrinsic surface states cannot exist at a metal-semiconductor interface and insisted that the pinning of the Fermi levels was due to metal-induced gap states (MIGS), which are composed of the tails of metal wave functions decaying into the semiconductor.[3] In 1976, using local-density formalism to calculate the Al/Si(111) interface, Louie and Cohen showed for the first time that a high density of MIGS's is formed in the band gap of the semiconductor.[4] Today, the MIGS pinning model has been developed further,[5,6] and seems to explain the SB formation of the covalent semiconductor.[7]

The chief obstacle to determining how SB's form is the obscurity of the atomic structure of the metal-semiconductor interface. A well-defined interface is needed to clarify the relationship between SBH and other physical parameters. Metal silicide–silicon interfaces are good for this. $NiSi_2$ and $CoSi_2$, which have fluorite structures with lattice constants close to that of silicon, are grown epitaxially on a Si(111) surface, and form atomically abrupt, structurally perfect interfaces. These interfaces have two types of structure. Type-*A* silicide has the same orientation as the Si substrate, and type-*B* silicide is rotated 180° about the Si⟨111⟩ axis. Tung *et al.* showed that both types of epitaxial layer can be grown on a Si(111) surface by carefully controlling the deposited Ni templates.[8] A thin template (1–7 Å) forms a type-*B* interface and a thick one (16–20 Å) forms a type-*A* interface after annealing at about 500 °C. Tung discovered that the SBH's in these $NiSi_2$/Si(111) interfaces differ.[9] This suggests a correlation between SBH and certain details of the interface atomic structure. While Tung's discovery is very important and seems to answer many questions, it is still debated. For example, Liehr *et al.* insist that there is no difference in the SBH's of type-*A* and type-*B* interfaces.[10] The difference in the SBH's has been experimentally confirmed to some extent,[11] but some still doubt the perfection of the interfaces and hypothesize that the difference in the SBH's is due to defects or other disorders at the interfaces.[12]

To explain the observed SBH difference, the detailed electronic structures must be examined with the first-principles calculations. Model theories or empirical calculations cannot accurately describe the small difference between the two structure types, because they apply parameters derived only from the bulk properties of the two constituents forming the interface.

We studied the electronic structures of the $NiSi_2$/Si(111) interfaces using the self-consistent linear muffin-tin orbitals method in the atomic-sphere approximation (LMTO-ASA), and obtained different SBH's for the two structure types, which is consistent with Tung's discovery. We briefly reported our results in a previous article.[13]

Soon after our work, Das, Blöchl, Christensen, and Andersen reported similar results.[14] Their results agreed qualitatively with ours, but showed some discrepancy. To resolve the differences, we performed calculations with different conditions. In this paper, we detail our calculations, and discuss their physical meaning and the accuracy of LMTO-ASA.

II. CALCULATIONS

We performed scalar relativistic calculations based on the Kohn-Sham density-functional formalism.[15] The

 ©1990 The American Physical Society

local-density approximation (LDA) is used for exchange and correlation with the parameters of Janak, Moruzzi, and Williams.[16] There are some kinds of representations of the LMTO basis.[17] We used the nearly orthogonal representation, and did not include the combined correction.

In LMTO-ASA calculations, the choices of atomic-sphere radius and position affect both band dispersion and total energy. Since there is no definite principle to determine the sphere radii, we performed nonrelativistic bulk band calculations and compared the band structures of bulk Si and $NiSi_2$ with those obtained by the full-potential linear augmented plane-wave method (FLAPW), which currently gives the most reliable electronic structure. The LMTO calculation for the Si band structure, especially for the occupied states, agreed well with the FLAPW result.

The $NiSi_2$ band dispersion differed somewhat when equal atomic-sphere radii were used for Si, Ni, and the empty sphere. With LMTO, the Γ_2^- point was 0.3 eV higher than the Fermi energy,[18] but with FLAPW the Γ_2^- point was 0.2 eV lower.[19] To resolve the discrepancy we determined sphere radii to agree with the FLAPW result. With these radii and *s*, *p*, and *d* orbitals, the Γ_2^- point became 0.05 eV lower than the Fermi energy. The highest discrepancy between LMTO and FLAPW was 0.3 eV for occupied bands. When the Ni sphere radius was 5% larger than the chosen value, the Fermi energy still remained 0.03 eV above the Γ_2^- point, and the band dispersion changed only slightly. As for the density of states, the antibonding peak just above the Fermi energy of $NiSi_2$ was at a slightly lower energy with the chosen radii than with the equal radii.

In the semirelativisitic calculation, the Γ_2^- point of bulk $NiSi_2$ was also 0.13 eV above the Fermi energy with equal sphere radii, and 0.23 eV lower than the Fermi energy with the chosen radii.

We used superlattice geometry with m Si_2 layers and n $NiSi_2$ layers in a unit cell. Calculations were made for four cell sizes: $m/n = \frac{3}{2}, \frac{6}{5}, \frac{9}{8}$, and $\frac{12}{11}$. These supercells had the same space group symmetry: D_{3d}^3. The largest $\frac{12}{11}$ supercell contained 93 atomic spheres: 46 Si, 11 Ni, and 36 empty spheres.

The lattice mismatch between Si and $NiSi_2$ is only 0.4%. Although x-ray standing waves suggest that the interface Si—Si bond contracts by about 0.1 Å within the limits of experimetal error,[20] we assumed that the lattice relaxation effect on SBH is the same for the two structure types.[21] We neglected lattice relaxation and used the Si lattice constant 5.429 Å. The $\frac{12}{11}$ supercell consisted of two thick regions: a 37.6-Å Si region and A 35.3-Å $NiSi_2$ region.

In the type-*A* structure the atomic spheres are placed in bcc sphere packing. In the type-*B* structure the empty spheres at the interface are placed to fill the interstitial region at equal distance from the interface atoms (Fig. 1). Although the bulk atomic-sphere radii are determined so as to agree with FLAPW, the interface empty-sphere radii are not uniquely determined. We chose interface empty-sphere radii which decrease the overlap between

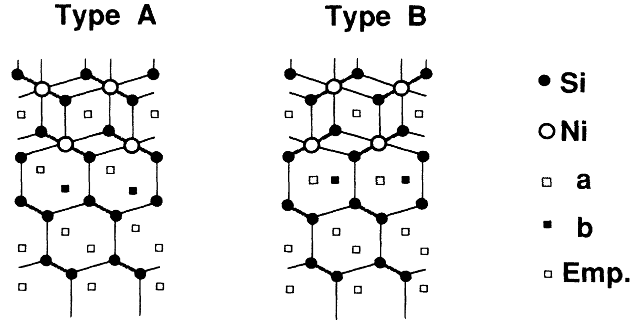

FIG. 1. Atomic structures of the two types of $NiSi_2$/Si(111) interface. Squares denote the positions of empty spheres. Empty spheres at the interfaces (*a*, *b*) are emphasized.

the spheres.

To get the most accurate self-consistent potential, we used a maximum of 162 nonequivalent **k** points in the first Brillouin zone of the supercell. First, we performed self-consistent iterations with only 16 **k** points. When the potential neared convergence, we increased the number of **k** points and iterated calculations to obtain the final self-consistent potential.

We used the self-consistent potential of a small supercell as the initial potential of a large supercell. For the $\frac{12}{11}$ supercell, the initial potential obtained from the $\frac{9}{8}$ supercell was very close to the final self-consistent potential, but it needed more than 100 iterations to converge. With large supercells, potential convergence becomes more unstable. Consequently, the mixing parameter, which determines the ratio of the new potential to the old potential during the iterations, must be smaller than a few percent.

III. RESULTS

Figure 2 shows the local density of states (LDOS) obtained from each layer of a $\frac{12}{11}$ supercell.[22] The LDOS agrees well with the bulk $NiSi_2$ density of states (DOS) in the $NiSi_2$ layer farthest from the interface, and the large *d*-electron peak is shifted to a higher energy near the interface in the $NiSi_2$ layers. In the farthest Si layer, the Si thermal gap almost appears, and the LDOS also agrees well with the bulk Si DOS. In the Si layers near the interface, the sharp peak at -7 eV and the small dip at 3 eV disappear. The arrows in Fig. 2 indicate interface states, which are formed mainly by *d* orbitals of the interface Ni atoms, and by Si *p* orbitals in the Si layers. More detailed discussions about the LDOS are given in a later section.

From our calculations with the larger supercells, we can determine the band lineup between the Si and $NiSi_2$ layers by examining the wave-function weights of the energy eigenvalues of the supercells in each atomic sphere of the Si and $NiSi_2$ layers. In a supercell having D_{3d}^3 symmetry, the valence-band bottoms (E_b) of both the Si and the $NiSi_2$ layers appear at the Γ_1^+ point and the valence-band maximum (E_v) of the Si layer appears at the Γ_3^+ point. Since we did not include the spin-orbit in-

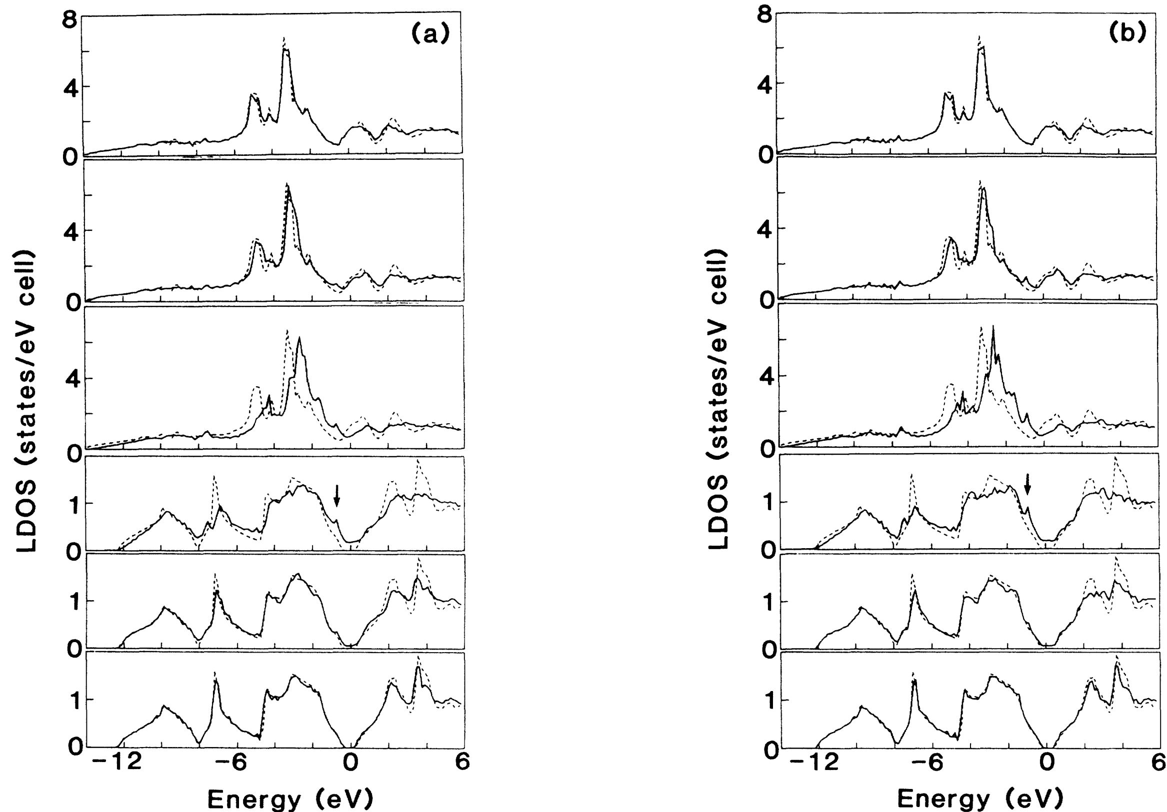

FIG. 2. Local density of states (LDOS) of the $NiSi_2$/Si(111) interface obtained with $\frac{12}{11}$ supercells: (a) of the type-A interface, (b) of the type-B interface. From top to bottom, they are sixth $NiSi_2$ layer, second $NiSi_2$ layer, first $NiSi_2$ layer, first Si_2 layer, second Si_2 layer, and sixth Si_2 layer from the interface. The dotted lines are bulk density of states of Si and $NiSi_2$. The arrows indicate interface states. The zero energy point indicates the Fermi energy of the supercell.

teraction, E_v of bulk Si has threefold degeneracy, but with the supercells, E_v is doubly degenerate.

In the two-dimensional hexagonal Brillouin zone of the supercell, the conduction-band minimum (E_c) of the Si layer appears at a location 0.875 of the way toward the M point along the Γ-M line, on which the Γ-X line of bulk Si is projected. Since the supercell is of finite size, there remains energy dispersion along the k_z direction (perpendicular to the interface). We searched for E_c by examining the wave functions of the eigenstates at the location 0.875 of the way along the Γ-M line, including those in the k_z direction. In each supercell, E_c of type A was at the $k_z=0$ point and E_c of type B was at the point whose k_z is the Brillouin-zone boundary. As k_z increases from zero to the Brillouin-zone boundary, the lowest-energy levels of the Si conduction band rise 0.005 eV for type A, and fall 0.007 eV for type B in $\frac{12}{11}$ supercells. This energy dispersion amounted to about 0.01–0.03 eV in $\frac{6}{5}$ and $\frac{9}{8}$ supercells.

Using E_b, E_v, E_c, and the Fermi energy of the supercell E_F, we obtained the SBH's (in this paper, SBH always means E_F-E_v), the Si thermal gaps (E_g), the Si valence-band widths (E_w equals E_v minus E_b of the Si layer), and the $NiSi_2$ valence-band widths (E_w equals E_F minus E_b of the $NiSi_2$ layer) listed in Table I. From these values, we can obtain the entire band lineup of the valence bands of the Si and $NiSi_2$ layers (Fig. 3).

Bulk calculations indicate that the valence-band width of $NiSi_2$ is 14.08 eV, and that of bulk Si is 11.94 eV. The Si thermal gap is depressed to 0.55 eV by the local-

TABLE I. Calculated Schottky-barrier height (E_F-E_v), thermal gap of Si layer (E_g), valence-band width of Si layer (E_w of Si), and valence-band width of $NiSi_2$ layer (E_w of $NiSi_2$) obtained from energy eigenvalues of supercells (in eV).

	$Si_2/NiSi_2$	$\frac{6}{5}$	$\frac{9}{8}$	$\frac{12}{11}$	Expt.[a]
E_F-E_v	Type A	0.48	0.34	0.38	0.47
	Type B	0.36	0.19	0.23	0.32
E_g	Type A	0.78	0.63	0.62	
	Type B	0.90	0.70	0.65	
E_w of Si	Type A	11.76	11.90	11.91	
	Type B	11.71	11.87	11.89	
E_w of	Type A	13.38	13.98	14.01	
$NiSi_2$	Type B	13.38	13.96	14.01	

[a]Reference 11.

density approximation although the experimental value is 1.17 eV. Since supercells are larger, E_g and E_w of both Si and $NiSi_2$ layers in Table I converge monotonically toward the calculated bulk values. However, the SBH's show different cell size dependence. SBH's oscillate with supercell sizes, although the oscillation becomes small as the supercell becomes larger. The difference between the SBH's of the two types is 0.15 eV in $\frac{9}{8}$ and $\frac{12}{11}$ supercells. This value is close to Tung's value 0.14 eV.

In Table I, SBH's, E_g, and E_w of both layers differ by more than 0.14 eV depending on the supercell size. However, the energy widths between E_F and E_b of the Si layer differ by only 0.06 eV with the supercell sizes (Fig. 3). The energy width between E_F and E_b of the Si layer differs only slightly between $\frac{6}{5}$ and $\frac{9}{8}$ supercells and the SBH's change by about 0.15 eV, because the valence-band width of the Si layer recovers to the bulk value. Between $\frac{9}{8}$ and $\frac{12}{11}$ supercells, the energy width between E_v and E_b of the $NiSi_2$ layer differs only slightly, so the SBH difference of 0.04 eV comes mainly from the change in the Fermi energy caused by the recovery of the valence-band width of the $NiSi_2$ layer. The calculated SBH's depend on the valence-band structures of both the Si and the $NiSi_2$ layers, especially in the neighborhood of the Fermi energy and Si band gap, but they do not depend so much on the valence-band bottom structures.

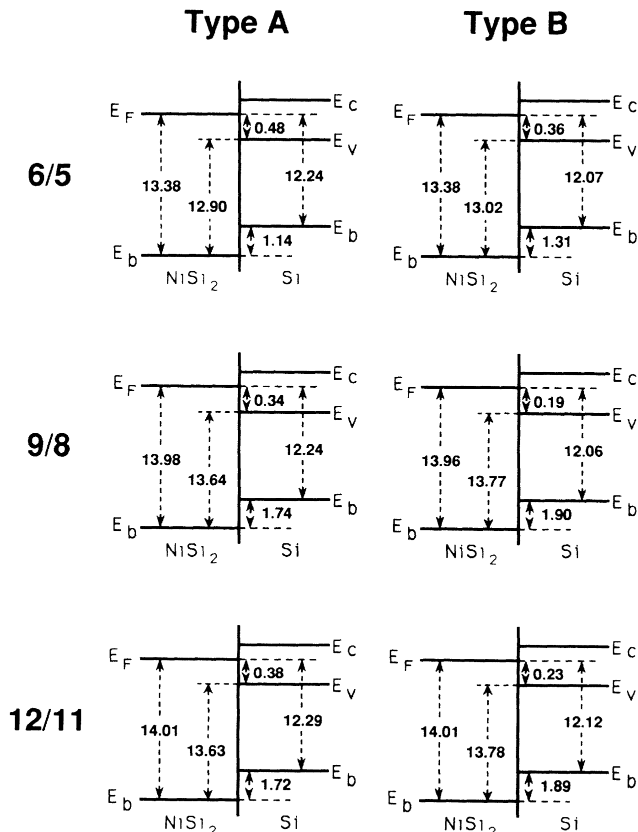

FIG. 3. The band lineup between the Si and $NiSi_2$ layers obtained with different supercells (in eV).

Table II lists the atomic-sphere radii and number of total electrons in each atomic sphere in bulk Si and $NiSi_2$. Figure 4 shows the difference in total number of electons from the bulk values for the $NiSi_2$/Si(111) interface obtained with $\frac{12}{11}$ supercells. In the Si layer, Si spheres close to the interface have fewer electrons than bulk Si, and the next empty spheres have more electons. Moving away from the interface, the deviation becomes small, but every Si sphere has fewer electrons than bulk Si and empty spheres have more electrons, so Si spheres are more positively charged than bulk Si and empty spheres are more negatively charged. Dielectric polarization occurs in the Si layer. The dipolelayer is composed of two Si atomic layers and two empty-sphere layers. The same dielectric polarization was also observed in our LMTO-ASA calculations for CaF_2/Si(111) interfaces.[23]

In the $NiSi_2$ layer, a charge oscillation occurs, which is different from the dielectric polarization in the Si layer. Although every Ni atomic spere has fewer electrons than bulk $NiSi_2$, the numbers of electrons in other spheres oscillate around the bulk values.

Two empty spheres at the interface are not included in Fig. 4. Their sphere radii and numbers of electrons are

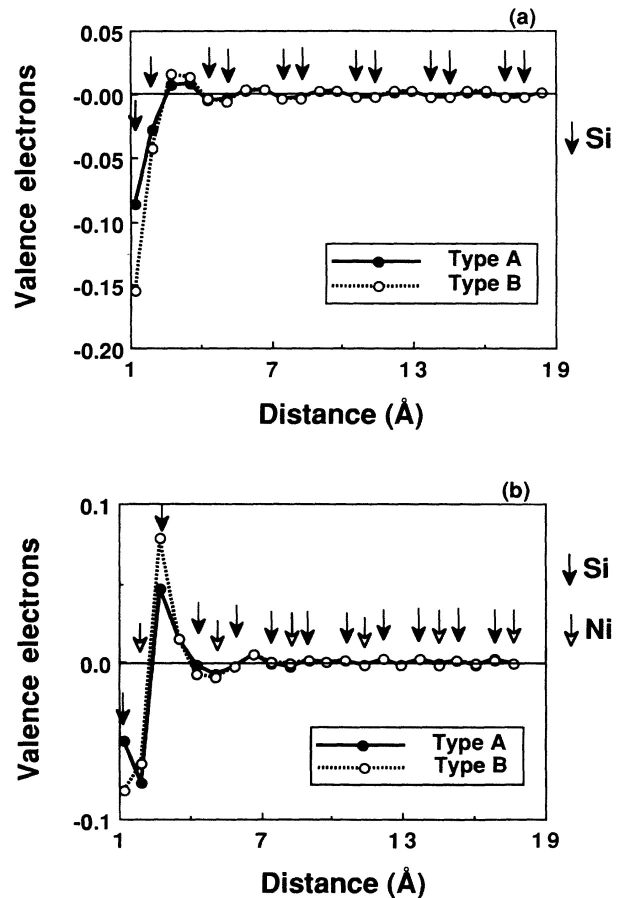

FIG. 4. Difference of the total number of electons from the bulk values in Table II: (a) in the Si layer, (b) in the $NiSi_2$ layer. The interface is on the left. Arrows indicate atomic-sphere locations.

TABLE II. Atomic-sphere radii and number of electrons of bulk Si and $NiSi_2$.

	Si		$NiSi_2$		
	Si	Empty	Si	Ni	Empty
Sphere radius (Å)	1.337	1.336	1.337	1.222	1.433
Number of electrons	13.214	0.786	13.218	27.730	1.833

listed in Table III. Spheres a and b have smaller electon densities than the empty sphere in $NiSi_2$. To understand the electron distribution at the interface, it is important to examine the atomic structure. In the Si layer, two Si spheres are located between empty spheres. In the $NiSi_2$ layer, the layer composed of one Ni and two Si spheres has empty spheres on both sides. There is additional space at the interface which is equal to about one-half the diameter of an empty sphere. To fill the additional space at the interface, electron transfer occurs. Consequently, there are fewer electrons in the interface spheres in both Si and $NiSi_2$ layers than bulk as is shown in Fig. 4.

All supercells have similar electron distributions, but the number of electrons in each sphere depends slightly on the supercell size. In $\frac{6}{5}$ and $\frac{9}{8}$ supercells, the difference in the number of electrons compared with the $\frac{12}{11}$ supercell is no more than 0.002 for each sphere, but in $\frac{3}{2}$ supercells this difference amounts to 0.01–0.02. The $\frac{3}{2}$ supercell does not have enough layers to screen out the interface disturbance produced by joining of the two different materials. The difference from the $\frac{12}{11}$ supercell is less in the $\frac{9}{8}$ supercell than in the $\frac{6}{5}$ supercell, and is greater in the $NiSi_2$ layer than in the Si layer for both types of interface.

IV. DISCUSSIONS

A. Schottky-barrier heights

Two other groups performed calculations on the two types of $NiSi_2$/Si(111) interface using LMTO-ASA. Bisi and Ossicini obtained SBH's which are 0 eV for type A and 0.3 eV for the type B in $\frac{3}{5}$ supercells.[24] The SBH difference between the two types is contrary to experimental evidence. Their LDOS shows a large peak near the Si conduction-band minimum in the interface layer, but this peak does not appear in our LDOS (Fig. 2). We cannot explain this discrepancy.

Das, Blöchl, Christensen, and Andersen reported on $\frac{6}{8}$ supercell calculations.[14] Their SBH's were 0.16 eV for type A and 0 eV for type B, using equal atomic-sphere radii in the $NiSi_2$ layers with LMTO-ASA. Their SBH's are smaller than ours. To resolve this discrepancy, we performed calculations for the type-A structure using equal radii for all atomic spheres as they did, and got a smaller SBH like theirs. The difference between our SBH's and theirs comes mainly from the choice of atomic-sphere radii.

We used supercell eigenvalues to calculate SBH's by examining wave-function weights in the Si and $NiSi_2$ layers. However, a different method for calculating SBH's from supercell calculations gives different values. Das *et al.* used self-consistent one-electron potentials obtained by supercell calculations. Their method yields the same SBH's as those obtained by the so-called "frozen-potential method."[25] By the frozen-potential method, one-electron potentials of the $NiSi_2$ and Si layers farthest from the interface are cut from the self-consistent potential obtained by supercell calculation, and exported to bulk band calculations, which yield the $NiSi_2$ Fermi energy (E_F') and the Si valence-band maximum (E_v'). We also used the frozen-potential approach and got the values of E_F' minus E_v' listed in Table IV. For every supercell size, E_F' minus E_v' values are smaller than the eigenvalue SBH's, and oscillate like the eigenvalue SBH's in Table I.

In the LDOS of Fig. 2, the dotted lines are bulk DOS's, which were drawn in the $NiSi_2$ layer for the bulk Fermi energy to coincide with the supercell Fermi energy. In the Si layer the bulk valence-band maximum was fitted to the eigenvalue E_v of the supercell. If the bulk Si DOS is fitted to the E_v' obtained by the frozen-potential method, the bulk DOS deviates more from the LDOS at the Si layer farthest from the interface. The LDOS is related to the eigenvalue E_v, but not to the frozen potential E_v'. This holds even with $\frac{9}{8}$ supercells. With $\frac{6}{5}$ supercells, however, bulk Si DOS was shifted to a much lower energy by this method because the eigenvalue SBH's are too large.

We reported different SBH's in our previous papers (Table V).[13] These were also obtained from the supercell eigenvalues, but calculation conditions were different from those that yielded the present results. Our previous calculations were nonrelativistic and used the frozen-core approximation and the $NiSi_2$ lattice constant of 5.406 Å. The present calculations are scalar relativisitic and use

TABLE III. Atomic-sphere radii and number of electrons of the empty spheres located at the interfaces (a and b in Fig. 1).

	Type A		Type B	
	a	b	a	b
Sphere radius (Å)	1.389	1.334	0.971	1.612
Number of electrons	1.102	0.780	0.315	1.630

TABLE IV. The difference between the $NiSi_2$ Fermi energy (E_F') and Si valence-band maximum (E_v') obtained by frozen-potential approach (in eV).

	$Si_2/NiSi_2$	$\frac{6}{5}$	$\frac{9}{8}$	$\frac{12}{11}$
$E_F'-E_v'$	Type A	0.41	0.32	0.36
	Type B	0.23	0.14	0.19

TABLE V. Schottky-barrier height obtained with different calculation conditions as described in the text (in eV).

	$Si_2/NiSi_2$	$\frac{6}{5}$	$\frac{9}{8}$	$\frac{12}{11}$
$E_F - E_v$	Type A	0.51	0.38	0.39
	Type B	0.45	0.29	0.33

the bulk Si lattice constant 5.429 Å, but the chief difference is the choice of empty-sphere radii at the interface (spheres a and b). In our previous calculations, we used the empty-sphere radius of $NiSi_2$ as the radius of one of the interface empty spheres. In the present calculations, we chose the interface empty-sphere radii to decrease the overlap between the spheres, as Das *et al.* did.

The previous SBH's showed a cell size dependence similar to that of the present SBH's (Table I). However, type B had SBH's about 0.1 eV larger than the present results. In the previous electron distribution on the Si side of type B, the second Si sphere from the interface had fewer electrons than that of Fig. 4(a).[26] This was caused by the large overlap between the sphere a and the second Si sphere. We think that the present calculations are better than the previous ones.

Although the choice of sphere radii affects the SBH values, SBH of type B is smaller than that of type A in every larger supercell. As is evident in Table I, the SBH values converge as the supercell size increases. Although the $\frac{12}{11}$ supercells are still too small to give conclusive SBH's, we speculate that final calculated SBH values will be within 0.04 eV of those of the $\frac{12}{11}$ supercells. The fact that the calculated SBH is lower than the experimental value is probably due to the LDA error.

B. Electronic structure

At the $NiSi_2/Si(111)$ interface, the interface Ni atoms have sevenfold coordinations in contrast to the eightfold coordinations in bulk $NiSi_2$.[27] These imperfect bonds cause the interface states near the Si thermal gap. In the LDOS of Fig. 2, the large d-electron peaks in the $NiSi_2$ layers near the interface are shifted to a higher energy. The same phenomena were also observed in calculations for $CoSi_2/Si(111)$ interfaces.[26] The energy shift appears when the interface Ni or Co atoms have semidangling bond states of $3d$ electrons in the sevenfold or fivefold interface structures.

The interface states of $NiSi_2/Si(111)$ are below the Fermi energy and are occupied by electrons. This is consistent with the simple picture given by van den Hoek *et al.*, which explains why interface structures differ for the $NiSi_2/Si(111)$ and $CoSi_2/Si(111)$ interfaces.[28] The main reason is that the Ni atom has one more electron than the Co atom.

In bulk $NiSi_2$, the quasigap separating the bonding and antibonding states is slightly below the Fermi energy.[29] In the $NiSi_2$ layers near the interface, the antibonding peak just above the Fermi energy has a lower density than bulk $NiSi_2$. Since the interface states appear just below the Fermi energy, the quasigap seems to be shifted up in energy.

Figure 5 shows the two-dimensional band structure near the Si band gap of the type-A interface. The zero energy point corresponds to the Fermi energy of the supercell. Each dot represents the energy eigenvalue of a $\frac{12}{11}$ supercell at the **k** point whose k_z element equals zero. The larger dots are eigenvalues whose wave functions exist in the Si layer more than 40%. The Si band is clearly distinguishable. The partial band gap of $NiSi_2$ can be seen near the M-K line in the Si band gap. The interface states appear in the partial band gap of $NiSi_2$.

In the LDOS of Fig. 2, the interface state of type B is at a lower energy than that of type A. In the two-dimensional band structure, its energy dispersion in the partial gap of $NiSi_2$ was slightly different from that of type A. Since the interface states are caused mainly by interface bonding configurations, this difference probably comes from the local atomic structures at the interface. The main structural difference between the two types is that the distance between the interface Ni atom and the second Si atom on the Si side is smaller in type B than in type A. From these facts, we speculate that bonding interaction exists between these atoms in type B, so that the interface states of the two types of interface have different energy dispersions.

Figure 6 shows the LDOS of the interface Si_2 layer of type A obtained with $\frac{3}{2}$, $\frac{6}{5}$, and $\frac{9}{8}$ supercells. In the $\frac{3}{2}$ supercell, the LDOS is rough compared with those of other supercells and the interface states are note easily distinguishable. The Si valence-band bottom of the $\frac{3}{2}$ supercell is at an energy about 0.3 eV higher than that of other supercells. The $\frac{3}{2}$ supercells are too small for the interface electronic structures to be examined.

Since there are two interfaces in a unit cell with supercell geometry, the tails of the interface states interact in the Si layer, so that the interface states of the $\frac{6}{5}$ supercell are slightly different from those of the $\frac{9}{8}$ supercell.[23] The LDOS of the $\frac{9}{8}$ supercell's interface Si_2 layer is almost the

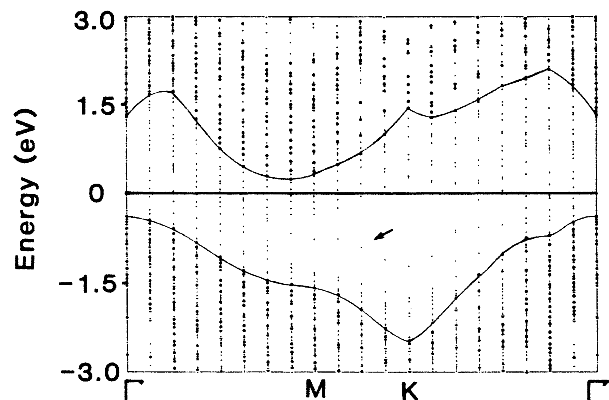

FIG. 5. Two-dimensional band structure near the Si band gap of the type-A interface. The zero energy point is the Fermi energy of the supercell. Each dot presents an energy eigenvalue. The larger dots indicate the eigenvalues whose wave functions exist in the Si layer more than 40% of the whole. The interface state is indicated by an arrow.

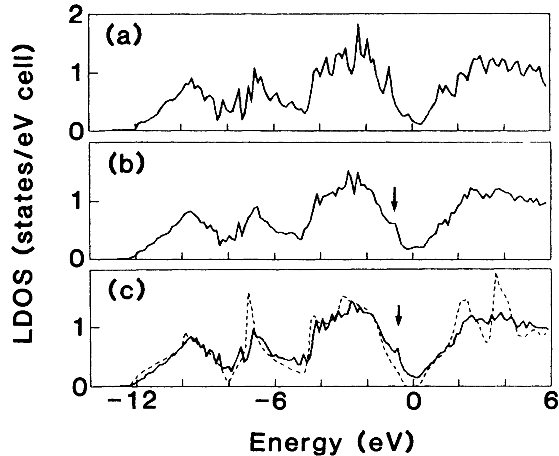

FIG. 6. Local density of states of first Si_2 layer from the interface of type A calculated (a) with $\frac{3}{2}$ supercell, (b) with $\frac{6}{5}$ supercell, (c) with $\frac{9}{8}$ supercell. The dotted line is bulk density of states of Si. The zero energy point is the Fermi energy of the supercells.

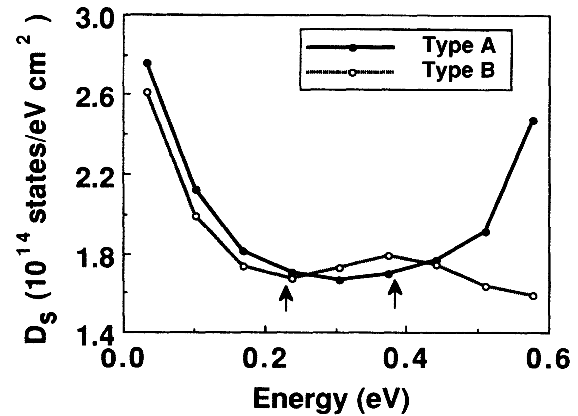

FIG. 7. Surface density of metal-induced gap states in the Si thermal gap. Arrows indicate the Fermi energies of the two types of interface. Circles show calculated energy points. By LDA, the Si thermal gap is depressed to about 0.6 eV (see Table I).

same as that in the $\frac{12}{11}$ supercell in Fig. 2. Type B showed almost the same LDOS dependence on cell size.

As was stated in the preceding section, SBH seems to depend on the valence-band structures in the neighborhood of the Fermi energy. Although the LDOS's in Fig. 2 for the two types of interface are very similar, the difference can be seen around the Fermi energy in addition to the difference of the interface states. In the Si layers, LDOS in both valence and conduction band decrease differently for the two types, especially near -3 and $+2$ eV. This probably concerned with SBH's.

C. Metal-induced gap states

In Fig. 2, the Si band gap is occupied by extra states called metal-induced gap states (MIGS). MIGS's are important for studying the metal-semiconductor interface. Figure 7 shows MIGS density (D_s) in the Si thermal gap. It was obtained from the $\frac{12}{11}$ supercells by summing up the LDOS between E_v and E_c of all the spheres in the Si layer except the two interface spheres, a and b. Although the MIGS in the Si thermal gap depends slightly on the supercell size, their density is more than 10^{14}/eV cm^2 in every supercell.

Figure 8 shows that space distribution of the total MIGS's in the Si layer. The perpendicular axis indicates the number of electrons which stay in each sphere if they occupy all MIGS's between E_v and E_c. Since the Fermi level is above E_v, more than half of the MIGS's are occupied by elelctrons. The MIGS's are mainly formed by Si p orbitals and are concentrated in the Si spheres rather than in the interstitial spheres, in contrast with the total valence electron distribution in the Si layer (Fig. 4). The MIGS's are formed of the states which are taken from the valence- and conduction-band states of the Si layer. This is why metal wave functions can penetrate deep into the Si layer even in the Si band gap, and a high density of MIGS's is formed.

D. Interface dipole

In LMTO-ASA, one-electron potential consists of spherical potentials at each atomic- and empty-sphere site. The spherical potential is composed of two different contributions. One comes from the charge distribution inside its own sphere, and the other is long-range (intersphere) electrostatic potential produced by surrounding spheres. The charges are treated as point charges placed at the sphere centers to calculate the intersphere electrostatic potential, whose on-site value is calculated by summing up the products of the Madelung constants and the point charges of the other spheres.

In Fig. 9 we plotted the intersphere electrostatic potential at each Si site in a $\frac{12}{11}$ supercell. It changes only near the interface and is rapidly screened. Comparing it with the electron distribution in Fig. 4, we recognize a large interface electric dipole layer with a positive layer on the

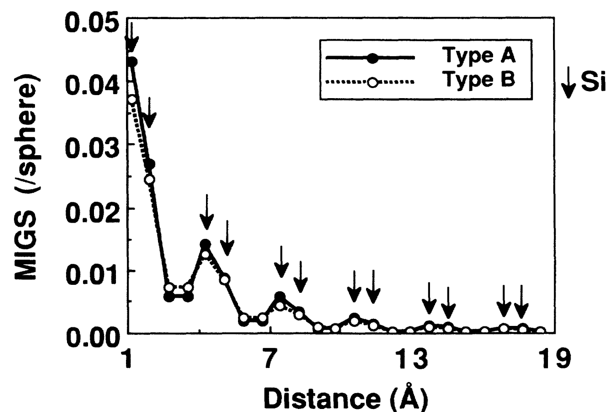

FIG. 8. Number of electrons obtained by integrating the density of metal-induced gap states in the Si thermal gap at each sphere. Arrows indicate Si locations.

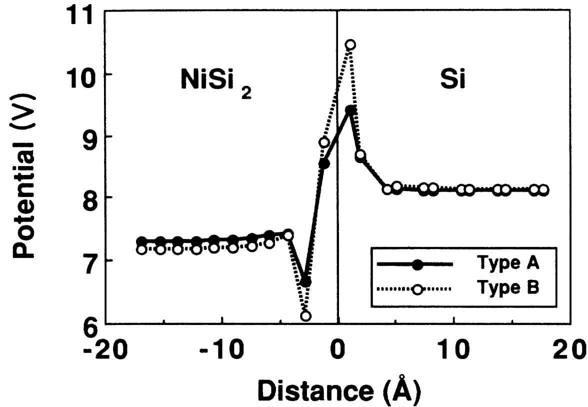

FIG. 9. Potential in each Si site. This was calculated by Madelung constants and charges in other atomic spheres. The center line is the interface.

Si side and a negative layer on the $NiSi_2$ side. On the Si side, the potential for type B is slightly larger than that for type A. On the $NiSi_2$ side, the potential for type B is smaller than that for type A. It almost reflects the SBH difference between the two types of interface, because type A has a smaller E_v in the Si layer and a larger E_F in the $NiSi_2$ layer than type B.

At the interface site, the potential differs by about 1 V for the two types, but the SBH differs by only 0.15 eV. The interface disturbance depends heavily on the atomic structure, but is screened in two or three layers on both the Si side and the $NiSi_2$ side. $\frac{3}{2}$ supercells have almost this many layers. As was stated in a preceding section, the electron distribution changes only slightly among $\frac{6}{5}$, $\frac{9}{8}$, and $\frac{12}{11}$ supercells, because the interface disturbance is sufficiently screened in two or three layers. However, the SBH changes by 0.04–0.17 eV depending on the cell size. Since supercells contain more Si and $NiSi_2$ layers, both layers have more bulklike character. This affects the calculated SBH's. The supercell must contain many layers for the SBH to converge sufficiently.

Das *et al.* reported 0.05 eV SBH lowering including the contraction of the interface Si—Si bond length.[14] Details of interface atomic positions also affect the calculated SBH's. In Fig. 2, the LDOS difference between the two types can be seen around -3 and $+2$ eV in the Si layers near the interface. Since the calculated SBH depends both on the interface details and on the thickness of the Si and $NiSi_2$ layers, we speculate that how the wave functions continue through the interface affects SBH, especially the wave functions of the energy states in the neighborhood of the Si band gap and the Fermi energy.

If only the calculation results of the $NiSi_2$/Si(111) interface are examined, it is difficult to understand why the two types of interface have different SBH's. Since the $CoSi_2$/Si(111) interface has an eightfold structure, interface atomic structures of the $NiSi_2$/Si(111) and $CoSi_2$/Si(111) interfaces are different.[30] In our preliminary calculations for the $CoSi_2$/Si(111) interfaces, type A had a larger SBH than type B, as is true for the $NiSi_2$(111) interfaces.[26] The SBH difference between the two types probably comes from the different boundary conditions at the interface, such as whether the $NiSi_2$ layer is rotated or not rotated around the Si⟨111⟩ axis. Since the energy states lower than the Fermi energy are formed mainly of p and d orbitals, we speculate that the orientation of the $NiSi_2$ layer causes the different SBH's.

V. SUMMARY

We obtained SBH's from the eigenvalues of large supercells. Although SBH's depend on the choice of the atomic-sphere radii and supercell size, SBH of the type-A interface is larger than that of the type-B interface. This is consistent with Tung's discovery.

The cell size dependence of SBH's is caused mainly by the valence-bandwidth of both Si and $NiSi_2$ layers, when the supercell has enough layers to screen the interface disturbance. We speculate that the electronic structures in the neighborhood of the Si band gap and the Fermi energy of $NiSi_2$ play an important role in forming the different Schottky barriers for the two types of $NiSi_2$/Si(111) interface.

ACKNOWLEDGMENTS

We would like to thank R. T. Tung, P. J. van den Hoek, and J. H. Werner for helpful discussions. We thank J. H. Werner for advising us of the work by Das *et al.*, and are grateful to H. Ishikawa for his encouragement. This work was supported by the Grant-in-Aid for Scientific Research (01650510) from the Ministry of Education, Science, and Culture of Japan.

[1]W. Schottky, Z. Phys. **118**, 539 (1942).
[2]J. Bardeen, Phys. Rev. **71**, 717 (1947).
[3]V. Heine, Phys. Rev. **138**, 1689 (1965).
[4]S. G. Louie and M. L. Cohen, Phys. Rev. B **13**, 2461 (1976).
[5]C. Tejedor, F. Flores, and E. Louis, J. Phys. C **10**, 2163 (1977).
[6]J. Tersoff, Phys. Rev. Lett. **52**, 465 (1984); Phys. Rev. B **32**, 6968 (1985).
[7]For a review of the metal-semiconductor interface, refer, for example, to F. Flores and C. Tejedor, J. Phys. C **20**, 145 (1987).
[8]R. T. Tung, J. M. Gibson, and J. M. Poate, Phys. Rev. Lett. **50**, 429 (1983).
[9]R. T. Tung, Phys. Rev. Lett. **52**, 461 (1984).
[10]M. Liehr, P. E. Schmidt, F. K. LeGoues, and P. S. Ho, Phys. Rev. Lett. **54**, 2139 (1985).
[11]R. T. Tung, K. K. Ng, J. M. Gibson, and F. J. Levi, Phys. Rev. B **33**, 7077 (1986); R. J. Hauenstein, T. E. Schlesinger, T. C. McGill, B. D. Hunt, and L. J. Schowalter. J. Vac. Sci. Technol. A **4**, 860 (1986); M. Ospelt, J. Henz, L. Flepp, and H. von Kanel, Appl. Phys. Lett. **52**, (1988).
[12]W. Mönch, Phys. Rev. Lett. **58**, 1260 (1987); A. Kikuchi, Phys. Rev. B **39**, 13 323 (1989).

[13]H. Fujitani and S. Asano, J. Phys. Soc. Jpn. **57**, 2253 (1988).
[14]G. P. Das, P. Blöchl, N. E. Christensen, and O. K. Andersen, in *Metallization and Metal-Semiconductor Interfaces,* edited by I. P. Batra (Plenum, New York, 1988); G. P. Das, P. Blöchl, O. K. Andersen, N. E. Christensen, and O. Gunnarsson, Phys. Rev. Lett. **63**, 1168 (1989).
[15]P. Hohenberg and W. Kohn, Phys. Rev. **136**, B864 (1964); W. Kohn and L. J. Sham, *ibid.* **140**, A1133 (1965).
[16]J. F. Janak, V. L. Moruzzi, and A. R. Williams, Phys. Rev. B **12**, 1257 (1975).
[17]O. K. Andersen, Phys. Rev. B **12**, 3060 (1975); O. K. Andersen, O. Jepsen, and D. Glötzel, in *Highlights of Condensed Matter Theory,* edited by F. Bassani, F. Fumi, and M. P. Tosi (North-Holland, Amsterdam, 1985), p. 59; O. K. Andersen, O. Jepsen, and M. Sob, in *Electronic Band Structure and its Applications,* edited by M. Yussouff (Springer-Verlag, Heidelberg, 1987).
[18]W. R. L. Lambrecht, N. E. Christensen, and P. Blöchl, Phys. Rev. B **36**, 2493 (1987).
[19]Y. J. Chabal, D. R. Hamann, J. E. Rowe, and M. Schluter, Phys. Rev. B **25**, 7598 (1982).
[20]E. Vlieg, A. E. M. J. Fischer, J. F. van der Veen, B. N. Dev, and G. Materlik, Surf. Sci. **17**, 36 (1986).
[21]J. H. Werner, Appl. Phys. Lett. **54**, 1528 (1989).
[22]We made some mistakes in our previous papers (Refs. 13 and 26). LDOS of $NiSi_2$ layers was compared with a wrong bulk DOS of $NiSi_2$ obtained with equal atomic-sphere radii for Si, Ni, and empty spheres, so that the large *d*-electron peak of the supercells seemed to shift to a higher energy even in the $NiSi_2$ layer farthest from the interface. In Ref. 13, we missed the interface states.
[23]H. Fujitani and S. Asano, Phys. Rev. B **40**, 8357 (1989).
[24]O. Bisi and S. Ossicini, Surf. Sci. **189**, 285 (1987).
[25]C. G. van de Walle and R. M. Martin, Phys. Rev. B **35**, 8154 (1987); N. E. Christensen, *ibid.* **37**, 4528 (1988).
[26]H. Fujitani and S. Asano, Appl. Surf. Sci. **41/42**, 164 (1989).
[27]J. M. Gibson, R. T. Tung, and J. M. Poate, in *Defects in Semiconductors II,* Proceedings of the Materials Research Society Symposium, Boston, 1982, edited by S. Mahajan and James W. Corbett (North-Holland, New York, 1983), Vol. 14, p. 395.
[28]P. J. van den Hoek, W. Ravenek, and E. J. Baerends, Phys. Rev. Lett. **60**, 1743 (1988); Surf. Sci. **205**, 549 (1988).
[29]J. Tersoff and D. R. Hamann, Phys. Rev. **28**, 1168 (1983).
[30]D. R. Hamann, Phys. Rev. Lett. **60**, 313 (1988).